JVST A
Journal of Vacuum Science & Technology A

ARTICLE

pubs.aip.org/avs/jva

Low-temperature etching of silicon oxide and silicon nitride with hydrogen fluoride

Cite as: J. Vac. Sci. Technol. A 42, 063006 (2024); doi: 10.1116/6.0004019
Submitted: 28 August 2024 · Accepted: 22 October 2024 ·
Published Online: 18 November 2024

View Online Export Citation CrossMark

Thorsten Lill,[1,a] Mingmei Wang,[1] Dongjun Wu,[1] Youn-Jin Oh,[1] Tae Won Kim,[1] Mark Wilcoxson,[1] Harmeet Singh,[1] Vahid Ghodsi,[2] Steven M. George,[2] Yuri Barsukov,[3] and Igor Kaganovich[3]

AFFILIATIONS

[1]Lam Research Corp., 4400 Cushing Parkway, Fremont, California 94538
[2]Department of Chemistry, University of Colorado, Boulder, Colorado 80309
[3]Princeton Plasma Physics Laboratory, 100 Stellarator Road, Princeton, New Jersey 08543

[a]**Electronic mail:** thorsten.lill@lamresearch.com

ABSTRACT

Etching of high aspect ratio features into alternating SiO_2 and SiN layers is an enabling technology for the manufacturing of 3D NAND flash memories. In this paper, we study a low-temperature or cryo plasma etch process, which utilizes HF gas together with other gas additives. Compared with a low-temperature process that uses separate fluorine and hydrogen gases, the etching rate of the SiO_2/SiN stack doubles. Both materials etch faster with this so-called second generation cryo etch process. Pure HF plasma enhances the SiN etching rate, while SiO_2 requires an additional fluorine source such as PF_3 to etch meaningfully. The insertion of H_2O plasma steps into the second generation cryo etch process boosts the SiN etching rate by a factor of 2.4, while SiO_2 etches only 1.3 times faster. We observe a rate enhancing effect of H_2O coadsorption in thermal etching experiments of SiN with HF. Ammonium fluorosilicate (AFS) plays a salient role in etching of SiN with HF with and without plasma. AFS appears weakened in the presence of H_2O. Density functional theory calculations confirm the reduction of the bonding energy when NH_4F in AFS is replaced by H_2O.

Published under an exclusive license by the AVS. https://doi.org/10.1116/6.0004019

18 November 2024 23:19:49

I. INTRODUCTION

Silicon oxide and nitride are widely used in the manufacturing of memory and logic devices because of their dielectric properties, etching selectivity, and compatibility with silicon-based devices. Complicated 3D structures are constructed from these materials utilizing a variety of deposition and etching processes. In the manufacturing of 3D NAND flash devices, deposition of alternating layers of SiO_2 and SiN (ONON) and of a carbon hardmask film precedes reactive ion etching (RIE) of holes with high aspect ratios as shown in Fig. 1(a). Subsequent selective isotropic etching processes recess SiO_2 and SiN laterally. Since SiO_2 remains in the device as the dielectric that separates tungsten metal plates, damage caused by the high energy impact of ions during the HAR ONON etching must be removed. This step is currently performed by wet etching.

Targeted recessing of either the SiO_2 or SiN layer can create an undulating sidewall as shown in Fig. 1(b). It serves as a template for a shaped ONO charge trap layer. Concave charge structures can increase the electric field in the space region between cells and deteriorate cell-to-cell interference, while convex structures can increase the electric field in the cell center and degrade reliability. Therefore, the shape of the charge trap structure must be carefully balanced to optimize the performance.[1] Selective vapor etching of SiO_2 and SiN offers precise shape control and top to bottom uniformity. After the ONO charge trap layers and polysilicon channel are deposited, and the remaining gap is filled with SiO_2, the sacrificial SiN in the stack is removed in an isotropic etching process with hot phosphoric acid. This process suffers from repeatability challenges and raises environmental concerns. Selective vapor processes are therefore under consideration.

Etching of holes and trenches with high aspect ratios into ONON stacks is a critical technology for scaling of 3D NAND flash memory.[2] To accomplish aspect ratios of 100:1 and larger as required by the 3D NAND scaling roadmap, novel HAR RIE technologies are being developed. New processes must improve etching rates to meet cost targets, reduce aspect ratio dependent etching (ARDE), have excellent mask selectivity and morphology, and avoid profile shortcomings such as twisting, bowing, and noncircular cross sections.

Published under an exclusive license by the AVS

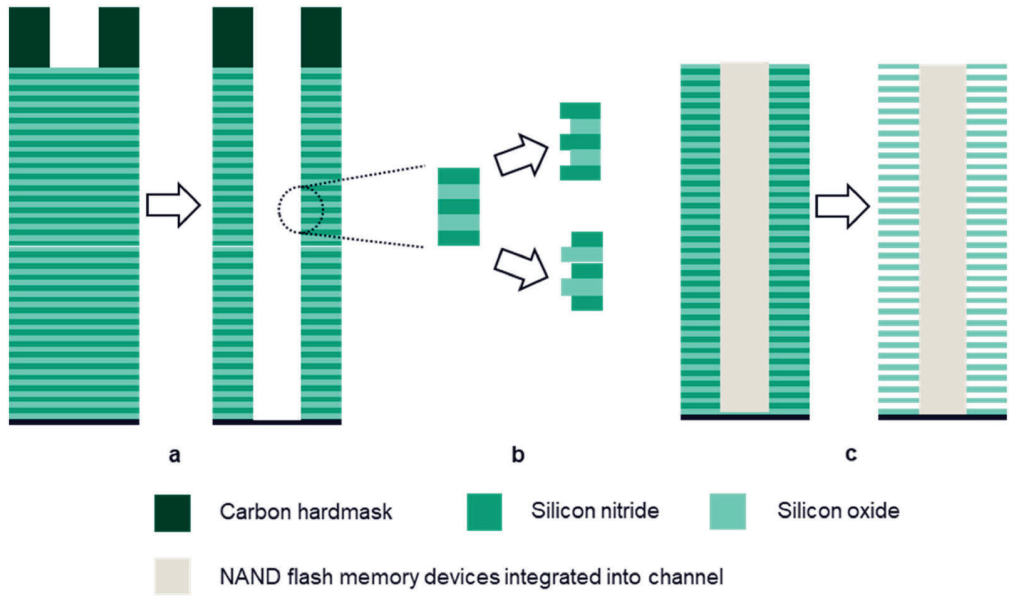

FIG. 1. Schematic illustration of existing and potential 3D NAND etching applications involving SiO_2 and SiN: (a) high aspect ratio etching of alternating SiO_2 and SiN to form holes into which NAND flash memory devices are vertically integrated. (b) Shaping of the ONON sidewall. (c) Removal of SiN to create cavities into which tungsten is later deposited.

Conventional HAR etching relies on the deposition of reactive C_xF_y polymer precursors at the etch front. Reactive polymer deposition strongly diminishes as the etching depth increases. For aspect ratios of 10 and beyond, the process is just chemical sputtering with negligible contribution from slow neutrals.[3] Lack of synergy between ions and neutrals limits the etching rate of conventional HAR processes. Because C_xF_y polymers are at the same time reactive and passivating layers, achieving high etching rates is impeded by clogging of the upper part of the profile. Polymer deposition also causes deterioration of mask morphology and hole shape.

The use of low wafer temperatures combined with new plasma chemistries can overcome these challenges.[4,5] Even though these processes do not operate at cryogenic temperatures of liquid nitrogen, they are colloquially referred to as "cryo" etching processes. In HAR cryo etching, the wafer temperature is low enough that process gases can physisorb at the surface. Novel, cryo etching specific gas mixtures change the reactive layer from "rich" C_xF_y polymers to a "lean" surface comprised of the etching material, hydrogen, and fluorine. The etching rates for these cryo etching processes are much higher than for conventional etching, which suggests that neutrals participate in the process.[4,5]

Three generations of high aspect ratio dielectric cryo etching processes have been reported to date.[6] Iwase *et al.* observed increased etching rates and reduced ARDE for SiO_2 and SiN for a gas mixture of HBr, N_2, and a fluorocarbon gas at a wafer temperature as low as 20 °C.[7] Shen *et al.* reported improved ARDE and mask morphology for a hydrogen and fluorine process and a pedestal temperature of −20 °C.[4] In this first-generation cryo process, hydrogen and fluorine are delivered independently as H_2 and a fluorine containing gas such as CF_4 or NF_3. Spectral analysis of a H_2/CF_4 plasma revealed the formation of HF which is known to etch SiO_2 spontaneously.[5] The concentration of HF can be increased when it is injected as feed gas. Average etching rates as high as 350 nm/min for 10 μm deep holes into ONON were achieved using a HF process at −60 °C pedestal temperature.[5]

Higher etching rates translate into lower cost, energy, and gas consumption. A review of publications on cryo etching over the last 30 years revealed that an increase in etching rate and reduction of ARDE is recurring observation which can be explained by enhanced physisorption of reactive gases.[8] Potential root causes for ARDE improvement are surface diffusion[8] and reduced charge up of the feature sidewall in the presence of HF and water on the surface.[9]

In this paper, we will focus on the second-generation ONON cryo HAR process which utilizes HF plasma. Additional experiments without plasma provide insight into potential neutral species contribution to this RIE process and at the same time offer dry etch solutions for the isotropic etching processes shown in Fig. 1. In the following, we will briefly summarize existing data on thermal and plasma etching of SiO_2 and SiN with HF and HF forming gas mixtures.

Thermal or vapor etching of SiO_2 with HF is an established process in semiconductor processing and micromachining. Early work relied on the presence of photoresist to initiate the reaction.[10,11] Miki *et al.* demonstrated thermal or vapor etching of SiO_2 with anhydrous HF at room temperature.[12] The addition of H_2O or alcohols reduces the incubation time, increases repeatability and etching rate.[13–15] Etching rates increase with decreasing

18 November 2024 23:19:49

Published under an exclusive license by the AVS

temperature for HF/methanol[16,17] and HF/H_2O gas mixtures in a multilayer adsorption regime.[18,19] Density functional theory (DFT) studies calculated activation energies of 0.72–0.79 eV for the four steps of fluorination of SiO_2[20] which is close to the 0.69 eV observed in experiments.[18] Molecular dynamics (MD) calculations utilizing a reactive force field (ReaxFF) predict a higher etching rate when the kinetic energy of HF impacting the SiO_2 surface is increased.[21] Hagimoto *et al.* exposed SiO_2 at 20–40 °C to a gas mixture of HF and NF_3 and observed the formation of $(NH_4)_2SiF_6$ or AFS which can be removed by surface heating in a second treatment chamber.[22] Junige and George demonstrated thermal etching of SiO_2 at 275 °C with a gas mixture of HF and NH_4, which was generated by heating of NH_4F to 130 °C.[23]

Etching of SiO_2 with low ion energy HF plasma has been demonstrated around the same time as gas only etching.[24] HF can be generated in hydrogen and fluorine containing plasmas. SiO_2 etching was demonstrated using NF_3/NH_3 remote plasma involving AFS formation.[25–27] AFS is formed on SiO_2 if the plasma contains fluorine, hydrogen, and nitrogen. It must be removed in a thermal or plasma step if the process temperature is below 120 °C. NF_3/NH_3 remote plasma processes are widely used in the semiconductor industry. They are better controlled than thermal etching of SiO_2 with HF which suffers from poor repeatability due to an incubation time.[14,28,29] Hidayat *et al.* published DFT calculations for NF_3/NH_3 remote plasma etching of SiO_2.[30] Their model assumes that HF and NH_4F are generated in the plasma and that NH_4F reacts with the SiO_2 surface to form AFS. Alternative remote plasma SiO_2 etching processes include SF_6/H_2, NF_3/H_2,[31] and HF/NH_3.[32] Gil *et al.* demonstrated etching of SiO_2 with H_2/NF_3 plasma and methanol vapor.[33]

Thermal etching of silicon nitride films was demonstrated using moist HF vapor followed by heating of the wafer[34] and HF aerosols.[35] The chemical processes, which occur when amorphous hydrogenated SiN reacts with HF, where studied with DFT.[36]

Knolle and Huttemann observed AFS on the surface of silicon nitride that had been hydrogenated and oxygenated prior to a CF_4 plasma treatment.[37] Hsiao *et al.* demonstrated the role of hydrogen in atomic layer etching (ALE) of SiN with CF_4/H_2 plasma via salt formation[38] and for continuous processing with CF_4/H_2 and HF/H_2 plasmas.[39] These results support the hypothesis that HF can spontaneously react with the hydrogenated SiN surface to form AFS. This salt must be removed from the surface to maintain etching either by heating the wafer or by exposure to plasma. AFS decomposes into NH_3, SiF_4, and HF when heated to temperatures of 100–120 °C.[19,33]

The formation of AFS is self-limited under certain conditions. This property can be utilized for ALE processes. Gill *et al.* realized SiN ALE where AFS was formed in a CH_2F_2/O_2/Ar remote plasma at −20 °C and removed using infrared lamp heating.[31] The etch-per-cycle (EPC) saturated at 1 nm/cycle when the exposure time was extended.[31] Shinoda *et al.* achieved an EPC of 2.6 nm/cycle using a hydrofluorocarbon remote plasma in one chamber and AFS removal on a heated pedestal in a separate chamber.[40]

Continuous etching of SiN was demonstrated for a range of fluorine and hydrogen containing remote plasmas such as CHF_3/O_2,[41] $CF_4/H_2/O_2$,[42] $NF_3/N_2/O_2/H_2$,[43] SF_6/H_2 and SF_6/D_2.[44] The dependence of the SiN etching rate on hydrogen flow was modeled considering vibrational excitation of HF.[43] The importance of vibrational excitation of HF was also demonstrated in experiments comparing HF and DF where the etching rate with DF was lower due to lower vibrational quantum energy.[44] AFS was absent when etching SiN with remote ClF_3/H_2 plasma which indicates that the presence of chlorine suppresses AFS formation while etching still occurs.[45]

II. EXPERIMENT

The experiments were carried out in three different reactors. Two of the reactors are commercial RIE tools, while the third reactor is custom built to study thermal etching. The reason for using two different types of RIE chambers was the availability of a liquid delivery system. Figure 2(a) shows an etching chamber with capacitively coupled plasma (CCP). This reactor has two radio frequency (RF) signals with 400 kHz and 60 MHz coupled to the cathode which is also equipped with a cooled electrostatic chuck (ESC). The ion energy in the experiments is about 5–6 keV and the

18 November 2024 23:19:49

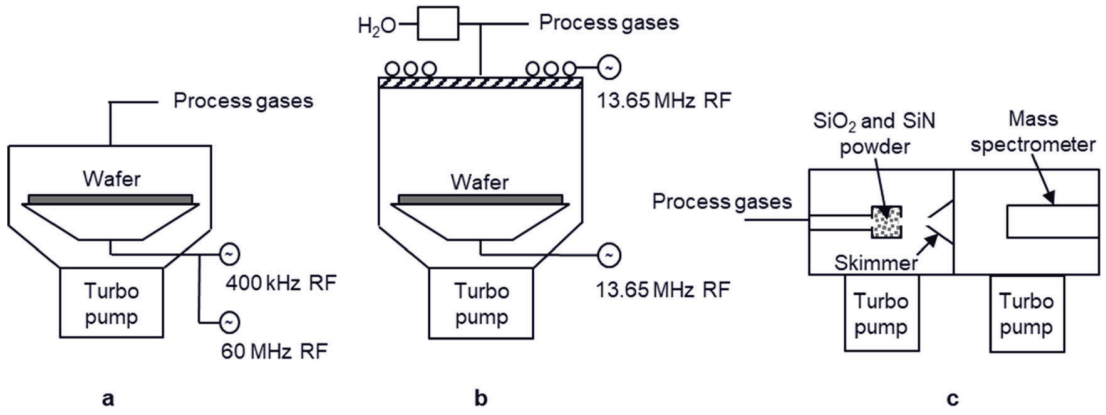

FIG. 2. Schematic illustration of the experimental reactors. (a) Dual frequency capacitively coupled plasma etching reactor. (b) Inductively couple plasma etching reactor. (c) Thermal etch reactor with powder sample and a mass spectrometer.

Published under an exclusive license by the AVS

ion flux is on the order of several $10^{16}/cm^{-2}$ s. The process gases enter the chamber through the top and are distributed evenly across the wafer with a showerhead. This included less commonly used gases such as HF and PF_3 which have low enough boiling points. The gap between the showerhead and the wafer is about 4 cm. The chamber has a turbo pump which maintains the process pressure in the millitorr range. This type of reactor is used in industrial high aspect ratio dielectric etching.

Experiments involving plasma and H_2O vapor were conducted in a chamber with inductively couple plasma (ICP) which features a vapor delivery system and a cooled ECS. The reactor is schematically illustrated in Fig. 2(b). The plasma is generated by an antenna which is energized by an RF signal with 13.56 MHz. The ions are accelerated by bias power applied to the cathode. The bias RF frequency is also 13.56 MHz. The gap between the dielectric window and the wafer is about 15 cm. The chamber has a turbo pump to support millitorr level process pressures. This chamber is not used for industrial HAR dielectric etching but serves as a chemistry test bed.

Figure 2(c) shows a schematic of the thermal etching experiment with a temperature-controlled reaction chamber and a chamber for *in situ* mass spectrometry analysis. This experimental setup was described in detail previously.[46] A first vacuum chamber contains the sample housing where SiO_2 and SiN powders are exposed to HF and H_2O. The gases are delivered by a stainless steel tube from the outside. They are diluted with nitrogen to carry the gas species. The sample housing is heated, and the temperature can be ramped. Volatile reaction products exit the sample housing through an aperture as a molecular beam that transports them through a skimmer and into a differentially pumped second chamber equipped with a quadrupole mass spectrometer (QMS). Detection of silicon containing species serves as a marker for etching.

We used blanket and patterned wafers in the experiments. The 300 mm blanket wafers were covered with 1000 nm PECVD tetraethyl orthosilicate (TEOS) SiO_2 and 2000 nm PECVD silane SiN. The patterned wafers were 1000 nm SiO_2, 1000 nm SiN and 6000 nm of alternating 40 nm SiO_2 and 40 nm SiN with 40 nm thickness. The mask was made of 2500 nm and 4000 nm PECVD carbon. The etching depth was measured using cross section scanning electron microscopy (SEM). The etched amount on the blanket wafers was determined with an optical thin film measurement tool. The powder from US Research Nanomaterials, Inc. used in the gas-only etching experiments was polycrystalline SiN (98%, 69–70 nm).

III. RESULTS AND DISCUSSION

Figure 3 shows an increased etching rate for a second-generation cryo etching process with HF as the main etching gas compared with a first-generation cryo etching process where HF is generated in a NF_3/H_2 plasma. The second-generation process also utilizes 5% PF_3 and other smaller amounts of additive gases with 5% or less of the total flow for profile control. The pedestal temperature was −20 °C which translates to a wafer surface temperature of about 10 °C due to the high ion flux and energy. The SEM micrographs show cross sections through circular holes etched for 300 s into the alternating SiO_2 and SiN films using the dual frequency CCP reactor shown in Fig. 2(a). The average etching rate for the second generation compared to the first generation more than

18 November 2024 23:19:49

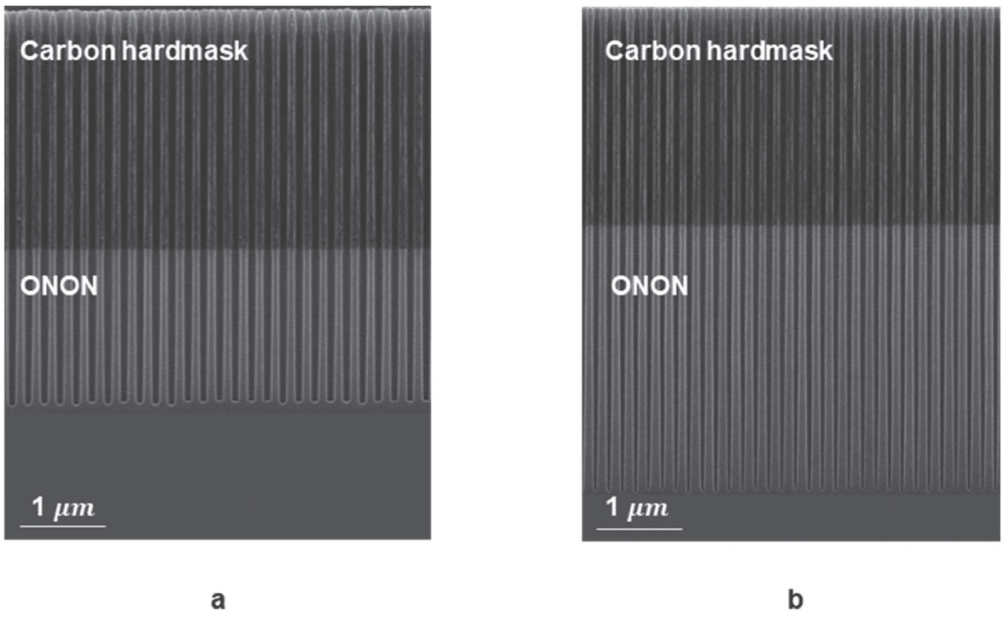

FIG. 3. SEM cross sections of holes etched into ONON stack in a dual frequency CCP reactor using two different recipes: (a) first-generation cryo etching recipe. (b) Second-generation cryo etching recipe.

Published under an exclusive license by the AVS

doubles from 310 to 640 nm/min for a final depth of 1500 and 3200 nm.

SiO_2 and SiN respond differently when changing from first- to second-generation cryo etching. Figure 4 shows experiments with patterned SiO_2, SiN, and ONON wafers, which were conducted in the CCP reactor. The etching times were 150 s for the first generation and 90 s for the second-generation cryo etching process. These times were chosen to account for the thinner SiO_2 film. An increase in etching rate for the second-generation cryo process is evident for all materials. The etching rate increases by a factor of 2.6, 1.6, and 1.9 for ONON, SiO_2, and SiN, respectively.

The effect of etching with HF instead of forming HF in the plasma is stronger for SiN compared to SiO_2. However, the effect is the strongest when etching SiO_2 and SiN simultaneously. One possible explanation is that the SiN profile has a sharp etch front for the second-generation cryo process which diminishes the etch rate of SiN. The etching rate of SiO_2 is lagging for the second-generation cryo process despite a flat etch front. This becomes even more pronounced when just HF without other gas additives is used. Adding PF_3 back into the process restores the etching rates. The addition of PF_3 quadruples the SiO_2 etching rate but increases SiN only by factor of 1.2. PF_3 has either a catalytic effect[5] or it provides additional fluorine which is needed to etch SiO_2.

The reaction of SiO_2 with HF generates gaseous SiF_4 and H_2O, which can be a gas or liquid depending on surface temperature and pressure,

$$SiO_2(s) + 4HF(g) \rightarrow SiF_4(g) + 2H_2O(l, g). \quad (1)$$

One approach to boost the SiO_2 etching rate is to lower the wafer temperature via accumulation of more H_2O at the surface. Temperature dependent normalized etching rates for SiO_2 and SiN are shown in Fig. 5. The etching rate of SiO_2 increases by 36% when cooling the wafer from 28 to −15.5 °C. It is known that

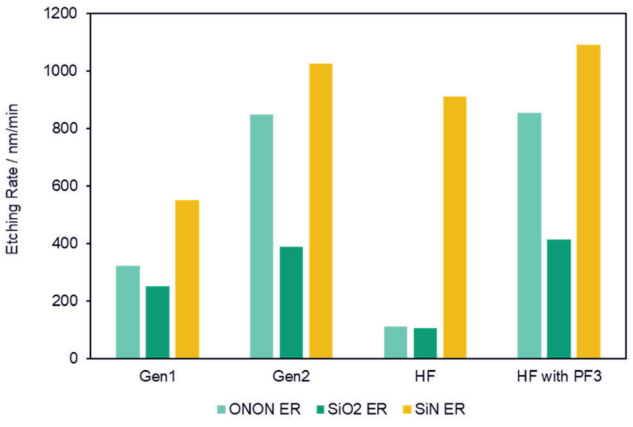

FIG. 4. Etching rates of SiO_2, SiN and stacks of alternating SiO_2/SiN (ONON) patterned with a carbon hardmask. Four different recipes were used. The setpoint of the chiller was −20 °C and the wafer temperature is estimated to be 10 °C.

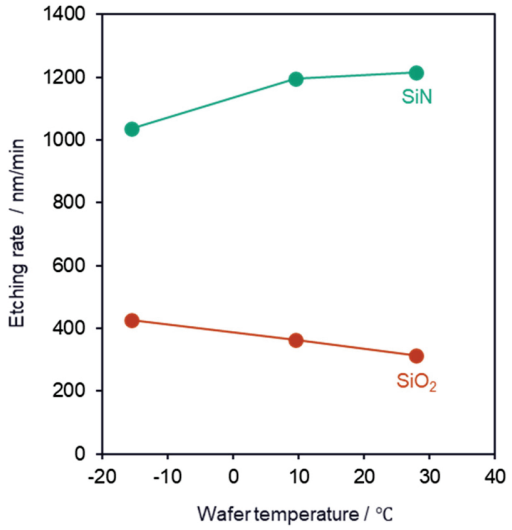

FIG. 5. Change in normalized etching rates of SiO_2 and SiN as a function of wafer temperature for a second-generation cryo etching recipe. The wafers were patterned with a carbon hardmask and the hole diameter was 100 nm. The final etched depth is about 1 μm. The experiments were conducted in a CCP reactor.

H_2O addition increases the etching rate of SiO_2 with HF vapor via a catalytic reaction.[15] H_2O is also formed as a product of the reaction as shown in Eq. (1). In contrast, the SiN etching rate decreases by 15% under these conditions. The SiN cross sections show tapered profiles with AFS sidewall residues at the lowest temperature.

To boost the SiO_2 etching rate further, we tested the effect of H_2O addition. Figure 6 shows the effect of water addition on the etching depth of ONON. We conducted the experiments with alternating HF and H_2O steps because mixtures of H_2O and HF are very corrosive. The experiments were conducted in the ICP chamber due to availability of the water vapor injection system. The etched depth increases by a factor of 1.5 for a sequence of 80 cycles of 5 s HF plasma and 2 s of H_2O plasma compared to 400 s HF plasma. The diameters of the holes were not changed by H_2O plasma, and the difference in the remaining mask was only 10% which eliminates changes in aspect ratio as a reason for the deeper etches. We also measured the etching rates with H_2O vapor steps without striking plasma. There was only a 17% effect on the ONON etching rate for a sequence of 80 cycles of 5 s HF plasma and 2 s of H_2O gas compared to 400 s HF plasma.

To identify the contributions of SiO_2 and SiN to the ONON etched depth increase, we conducted additional blanket wafer experiments. Figure 7 shows that the SiN etching rate benefits from water plasma step addition much more than SiO_2. The SiN etching rate increases by a factor of 2.4 for a sequence of 6 cycles of 5 s HF plasma and 2 s of H_2O plasma compared to 30 s HF plasma. For SiO_2, the etching rate increased only by a factor of 1.26.

18 November 2024 23:19:49

Published under an exclusive license by the AVS

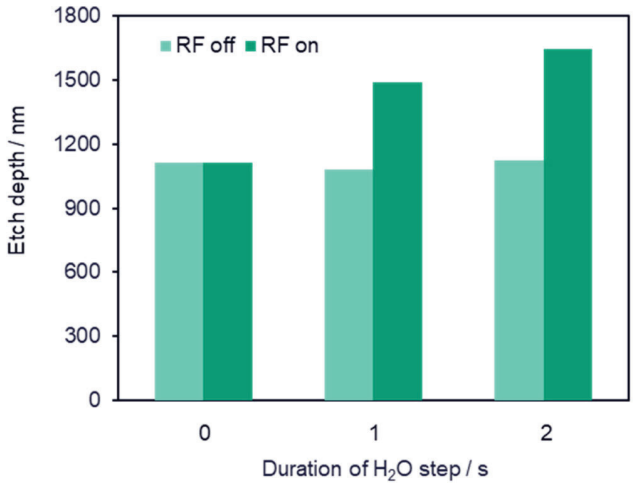

FIG. 6. Depth of holes etched into alternating silicon nitride and silicon oxide layers with HF plasma and intermittent H_2O steps with and without plasma. The wafers were patterned with a carbon hardmask. The experiments were conducted in an ICP reactor. The wafer temperature was 0 °C.

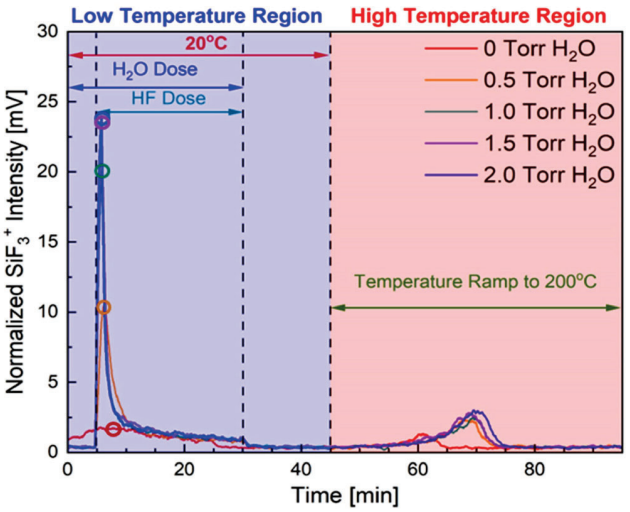

FIG. 8. Normalized SiF_3^+ signal of gaseous products from the reaction of SiN with HF and H_2O gases. The partial pressure of HF is 0.5 Torr. The sample was heated with a linear ramp to 200 °C after 45 min to evaporate AFS. The circles indicate the maximum value of the low-temperature peaks for different H_2O flows.

The effect of water plasma on SiO_2 is most likely the result of SiO_2 hydroxylation which has a catalytic effect on the surface reaction.[13,15] Exposure to HF plasma likely removes H_2O and hydroxyl surface groups and leaves a fluorinated surface. H_2O plasma restores the hydroxylated surface more effectively than H_2O vapor. Fluorine terminated SiO_2 surfaces are not readily hydrolyzed by exposure to water.[15] The catalytic effect of H_2O gas on etching of SiO_2 with HF gas may or may not involve the formation of a thin liquid water layer. Kang and Musgrave identified in DFT computations that gaseous H_2O can transfer a hydrogen atom to the hydroxyl group at the surface to form water and simultaneously accept hydrogen from HF. This leaves fluorine to attack to exposed silicon surface atoms.[15] If there is sufficient water at the surface, HF_2^- and H_3O^+ could form. HF_2^- is a critical driver for the wet etching rate of SiO_2.[47] The transition from gas to a liquid type of reaction mechanism is unknown which warrants future research. A recent report attributes a five-molecule water cluster liquidlike properties.[48] To boost the SiO_2 etching rate, mixing of HF and H_2O and lower wafer temperatures is a potential approach.

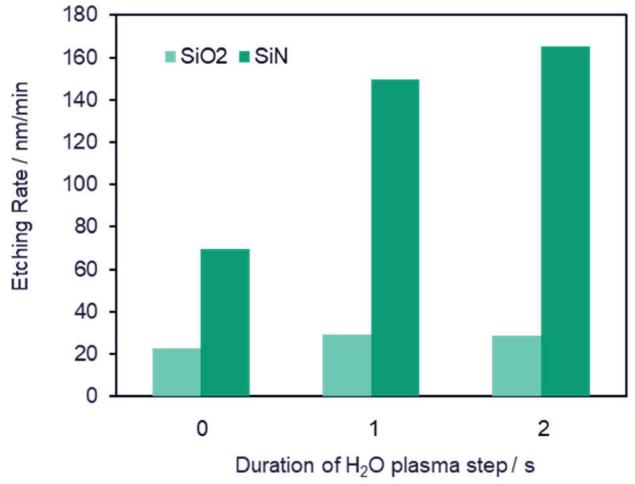

FIG. 7. Blanket etching rates of silicon oxide and silicon nitride etched with alternating HF and H_2O plasma steps. The experiments were conducted in an ICP reactor. The wafer temperature was 0 °C.

The effect of the water plasma on the SiN etching rate could be the result of implantation of hydrogen into SiN which is known to boost the formation of AFS at low temperatures.[39] H_2O can also oxidize the SiN surface and lead to the formation of AFS under exposure to fluorine containing plasmas.[37] A third potential explanation is weakening of AFS bonds in the presence of water. AFS is formed in the reaction between SiN and HF which can slow down etching. We use the stoichiometric composition of SiN in the following equation to reflect the general case:

$$Si_3N_4(s) + 16HF(g) \rightarrow 2(NH_4)_2SiF_6(s) + SiF_4(g). \quad (2)$$

When AFS is heated to a temperature over 100 °C, AFS decomposes into gaseous reaction products,[19,33]

$$(NH_4)_2SiF_6(s) \rightarrow 2NH_3(g) + 2HF(g) + SiF_4(g). \quad (3)$$

This decomposition reaction can also be activated by plasma which generates energetic ions, electrons, and photons. Weaker AFS bonds would promote the disintegration of AFS.

18 November 2024 23:19:49

Published under an exclusive license by the AVS

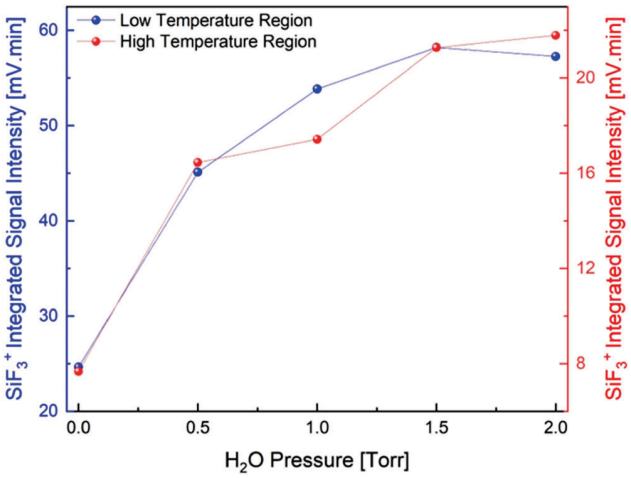

FIG. 9. Integrated SiF_3^+ signal of gaseous products from the reaction of SiN with HF and H_2O gas and from evaporation of AFS at elevated temperatures. The partial pressure of HF is 0.5 Torr.

To gain a better understanding of the chemical reactions between SiN, HF, and H_2O, mass spectrometry experiments were conducted in the thermal etch reactor as shown in Fig. 2(c). Figure 8 shows the SiF_3^+ signal originating from SiN exposed to 0.5 Torr HF and H_2O with variable partial pressure of H_2O at 20 °C. SiF_3^+ is the QMS fragmentation product of SiF_4 which is the main etch product that is released during exposure of SiN to HF according to Eq. (2) and of the AFS decomposition reaction in Eq. (3). Its signal serves as proxy of SiN etching rate. HF etches SiN spontaneously at room temperature at a pressure of 0.5 Torr. The addition of water increases the SiF_3^+ signal. The spontaneous etching rate decreases over time indicating that the surface is being covered with AFS. Ramping the temperature to 200 °C after turning off the HF and H_2O gas flows reveals the desorption of the AFS decomposition product at temperatures between 100 and 120 °C.

Figure 9 shows the integrated SiF_3^+ signals for the spontaneous low-temperature reaction and the high temperature AFS decomposition. Both curves saturate for a partial pressure of H_2O which is four times that of HF. This ratio could reflect how many H_2O molecules are needed to dissociate HF at the surface. The integrated signal corresponding to spontaneous etching is 2.75 times larger than the signal originating from AFS.

The increase of the signals for spontaneous etching and AFS can be explained by a catalytic effect of H_2O on the reaction of HF with SiN. Weakening of the AFS structure by water adsorption is an alternative explanation. For the reaction of HF with SiN to proceed, HF must diffuse to the AFS/SiN interface and SiF_4 must diffuse back to the surface. It is possible that AFS transforms into a saturated liquid solution in the presence of H_2O, which facilitates diffusion. In the presence of H_2O, it takes longer to build up passivating AFS while SiN is etching, and hence the SiF_3^+ signal is stronger. Since that the AFS/H_2O passivation layer is weaker, more AFS is needed to stop the etching and the AFS evaporation signal shows a similar partial pressure dependence as the etching signal.

The effect of H_2O on the molecule binding energy of AFS was studied with DFT using GAUSSIAN 16. An LC-wHPBE DFT functional was selected because it matched best experimental results for the binding energy of HF clusters published by NIST.[49] The results of these calculations for 0–4 H_2O molecules forming hydrogen bonds with a SiF_4 center are illustrated in Fig. 10. The starting point is SiF_4 bonded with two NH_4F molecules with a molecule binding energy of 0.47 eV. Substitution of NH_4^+ with H_3O^+ gives $(H_3O)(NH_4)SiF_6$ with a binding energy of 0.41 eV. Replacing another NH_4^+ with H_3O^+ yields $(H_3O)_2SiF_6$ with a binding energy of 0.35 eV. Two more water molecules can bond to this cluster via

18 November 2024 23:19:49

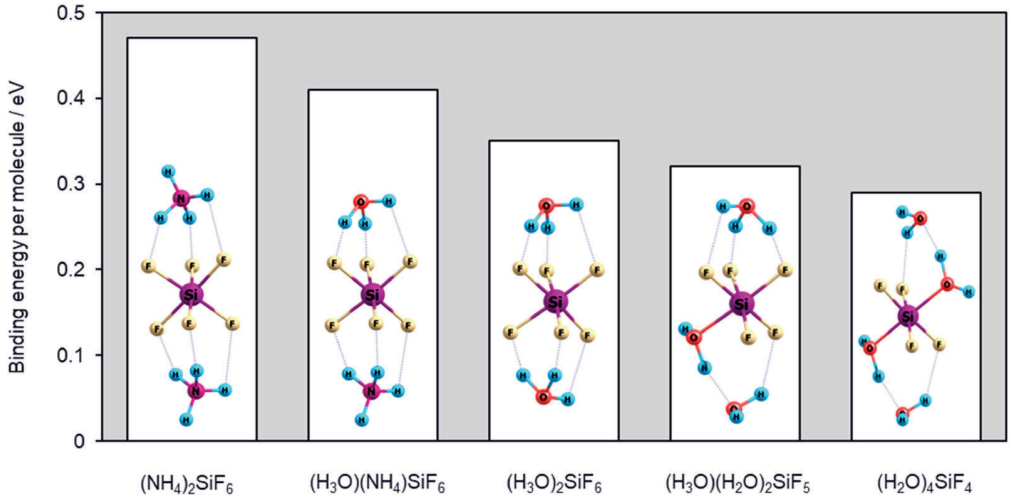

FIG. 10. Binding energies for $(NH_4)_2SiF_6$ with gradual replacement of NH_4 ligands by H_2O calculated with DFT.

Published under an exclusive license by the AVS

hydrogen bonds with oxygen and fluorine. Two HF molecules are removed in the process. The resulting $(H_3O)(H_2O)_2SiF_5$ and $(H_2O)_4SiF_4$ molecules have binding energies of 0.31 and 0.29 eV, respectively. These computational results corroborate the idea that exposing AFS to H_2O weakens the binding energies which could explain the higher spontaneous etching rates of SiN with HF gas in the presence of H_2O.

Our results indicate that increasing the H_2O concentration at the surface offers a promising path to further increase the etching rate for high aspect ratio ONON in second-generation cryo processes. While a strong enhancement of the SiN etching rate was demonstrated in our experiments, boosting the SiO_2 etching rate may require lower temperatures if AFS formation on SiN can be controlled.

IV. SUMMARY AND CONCLUSIONS

A second-generation cryo etching process with HF plasma etches ONON faster by a factor of 2.6 than the first-generation cryo process with separate gases as sources of fluorine and hydrogen at a pedestal temperature of −20 °C and a wafer surface temperature of around 10 °C. The etching rate increase is more pronounced for SiN compared to SiO_2. The observation that ONON etches faster than either SiO_2 or SiN is most likely caused by SiN profile tapering, which is caused by accumulation of AFS. More AFS is formed on SiN when the surface temperature is decreased leading to lower etching rates. The SiO_2 etching rate increases most likely due to enhanced adsorption of H_2O. Insertion of H_2O gas and plasma steps accelerates ONON etching. H_2O plasma is more effective than gas only and SiN exhibits a larger etching rate enhancement than SiO_2.

Thermal etching of SiN with HF is accelerated in the presence of H_2O. Both spontaneous etching and the formation of AFS are boosted. DFT calculations support the hypothesis that H_2O weakens the AFS layer, which inhibits etching of SiN.

Spontaneous etching can be a contributor to low-temperature HAR etching if HF can reach the etch front. It is important to provide enough ion energy to remove the AFS from the etch front. Chemical tuning knobs to balance AFS formation in addition to H_2O are important. The SiO_2 etching rate is limiting the overall rate for ONON etching. It can be boosted by fluorine addition and H_2O adsorption with the latter being more effective at lower temperatures.

ACKNOWLEDGMENTS

The authors would like to thank Shuai Lou and Qing Xu from Lam Research for their support of the reactive ion etch experiments. The DFT calculations were conducted under the Laboratory Directed Research and Development (LDRD) Program at Princeton Plasma Physics Laboratory, a national laboratory operated by Princeton University for the U.S. Department of Energy. In addition, this research used computing resources on the Princeton University Adroit Cluster and Stellar Cluster.

AUTHOR DECLARATIONS

Conflict of Interest

The authors have no conflicts to disclose.

Author Contributions

Thorsten Lill: Conceptualization (equal); Data curation (equal); Formal analysis (equal); Writing – original draft (equal). **Mingmei Wang:** Conceptualization (equal); Data curation (equal); Writing – review & editing (equal). **Dongjun Wu:** Data curation (equal); Investigation (equal); Methodology (equal). **Youn-Jin Oh:** Conceptualization (equal); Data curation (equal); Writing – review & editing (equal). **Tae Won Kim:** Conceptualization (equal); Writing – review & editing (equal). **Mark Wilcoxson:** Conceptualization (equal); Writing – review & editing (equal). **Harmeet Singh:** Conceptualization (equal); Data curation (equal); Project administration (equal); Resources (equal); Writing – review & editing (equal). **Vahid Ghodsi:** Conceptualization (equal); Data curation (equal); Formal analysis (equal); Investigation (equal); Visualization (equal). **Steven M. George:** Conceptualization (equal); Data curation (equal); Formal analysis (equal); Resources (equal); Supervision (equal). **Yuri Barsukov:** Conceptualization (equal); Data curation (equal); Formal analysis (equal); Investigation (equal); Methodology (equal); Software (equal); Visualization (equal); Writing – original draft (equal). **Igor Kaganovich:** Resources (equal); Supervision (equal); Writing – review & editing (equal).

DATA AVAILABILITY

The data that support the findings of this study are available within the article.

REFERENCES

[1]S. Park *et al.*, *IEEE Symposium on VLSI Technology Digest of Technical Papers 2021*, Kyoto 13–19 June, 2021 (IEEE, 2021).
[2]H. Singh, Solid State Technol. **60**, 18 (July 2017), see https://sst.semiconductor-digest.com/2017/07/overcoming-challenges-in-3d-nand-volume-manufacturing.
[3]S. Huang, C. Huard, S. Shim, S. K. Nam, I. C. Song, S. Lu, and M. J. Kushner, J. Vac. Sci. Technol. A **37**, 031304 (2019).
[4]M. Shen *et al.*, Jpn. J. Appl. Phys. **62**, SI0801 (2023).
[5]Y. Kihara, M. Tomura, W. Sakamoto, M. Honda, and M. Kojima, *IEEE Symposium on VLSI Technology Digest of Technical Papers 2023*, Kyoto, 11–16 June, 2023 (IEEE, 2023).
[6]Lam Research Press Release (July 2024), see https://newsroom.lamresearch.com/2024-07-31-Lam-Research-Introduces-Lam-Cryo-TM-3-0-Cryogenic-Etch-Technology-to-Accelerate-Scaling-of-3D-NAND-for-the-AI-Era.
[7]T. Iwase, K. Yokogawa, and M. Mori, Jpn. J. Appl. Phys. **57**, 06JC03 (2018).
[8]T. Lill, I. L. Berry, M. Shen, J. Hoang, A. Fischer, T. Panagopoulos, J. P. Chang, and V. Vahedi, J. Vac. Sci. Technol. A **41**, 023005 (2023).
[9]S. N. Hsiao, M. Sekine, K. Ishikawa, Y. Iijima, Y. Ohya, and M. Hori, Appl. Phys. Lett. **123**, 212106 (2023).
[10]R. L. Bersin, J. H. Junkin, and R. F. Reichelderfer, U.S. patent 4,127,437 (28 November 1978).
[11]D. F. Weston and R. J. Mattox, J. Vac. Sci. Technol. **17**, 466 (1980).
[12]N. Miki, H. Kikuyama, I. Kawanabe, M. Miyashita, and T. Ohmi, IEEE Trans. Electron Devices **37**, 107 (1990).
[13]C. R. Helms and B. E. Deal, J. Vac. Sci. Technol. A **10**, 806 (1992).
[14]K. Torek, J. Ruzyllo, R. Grant, and R. Novak, J. Electrochem. Soc. **142**, 1322 (1995).
[15]J. K. Kang and C. B. Musgrave, J. Chem. Phys. **116**, 275 (2002).
[16]C. S. Lee, J. T. Baek, H. J. Yoo, and S. I. Woo, J. Electrochem. Soc. **143**, 1099 (1996).
[17]T. Hattori *et al.*, Jpn. J. Appl. Phys. **62**, SI1001 (2023).

18 November 2024 23:19:49

Published under an exclusive license by the AVS

[18]Y.-P. Han, "HF vapor etching and cleaning of silicon wafer surfaces," Ph.D. thesis (Massachusetts Institute of Technology, 1999).
[19]S. M. George, private communication (2024).
[20]R. Hidayat, H.-L. Kim, K. Khumaini, T. Chowdhury, T. R. Mayangsari, B. Cho, S. Park, and W.-J. Lee, Phys. Chem. Chem. Phys. **25**, 3890 (2023).
[21]D. H. Kim, S. J. Kwak, J. H. Jeong, S. Yoo, S. K. Nam, Y. Kim, and W. B. Lee, ACS Omega **6**, 16009 (2021).
[22]Y. Hagimoto, H. Ugajin, D. Miyakoshi, H. Iwamoto, Y. Muraki, and T. Orii, Solid State Phenom. **134**, 7 (2007).
[23]M. Junige and S. M. George, Chem. Mater. **36**, 6950 (2024).
[24]G. Smolinsky, T. M. Mayer, and E. A. Truesdale, ECS J. Solid State Sci. Technol. **129**, 1770 (1982).
[25]H. Nishino, N. Hayasaka, and H. Okano, J. Appl. Phys. **74**, 1345 (1993).
[26]H. Ogawa, T. Arai, M. Yanagisawa, T. Ichiki, and Y. Horiike, Jpn. J. Appl. Phys. **41**, 5349 (2002).
[27]H.-T. Kim, J.-S. Lim, M.-S. Kim, H.-J. Oh, D.-H. Ko, G.-D. Kim, W.-G. Shin, and J.-G. Park, Microelectron. Eng. **135**, 17 (2015).
[28]J. Ruzyllo, K. Torek, C. Daffron, R. Grant, and R. Novak, J. Electrochem. Soc. **140**, L64 (1993).
[29]S. Guillemin, P. Mumbauer, H. Radtke, M. Fimberger, S. Fink, J. Kraxner, A. Faes, and J. Siegert, J. Microelectromech. Syst. **28**, 717 (2019).
[30]R. Hidayat *et al.*, J. Vac. Sci. Technol. A **41**, 032604 (2023).
[31]Y. J. Gill, D. S. Kim, H. S. Gil, K. H. Kim, Y. J. Jang, Y. E. Kim, and G. Y. Yeom, Plasma Process Polym. **18**, e2100063 (2021).
[32]N. Miyoshi, K. Shinoda, H. Kobayashi, M. Kurihara, Y. Kouzuma, and M. Izawa, J. Vac. Sci. Technol. A **40**, 012601 (2022).
[33]H. S. Gil, D. S. Kim, Y. J. Jang, D. W. Kim, H. I. Kwon, G. C. Kim, D. W. Kim, and G. Y. Yeom, Sci. Rep. **13**, 11599 (2023).
[34]G. Vereecke, M. Schaekers, K. Verstraete, S. Arnauts, M. M. Heyns, and W. Plante, J. Electrochem. Soc. **147**, 1499 (2000).
[35]H.-J. Kwon and J.-G. Park, J. Korean Phys. Soc. **81**, 903 (2022).
[36]K. Khumaini, Y. Kim, R. Hidayat, T. Chowdhury, H.-L. Kim, B. Cho, S. Park, and W.-J. Lee, Appl. Surf. Sci. **654**, 159414 (2024).
[37]W. R. Knolle and R. D. Huttemann, J. Electrochem. Soc. **135**, 2574 (1988).
[38]S.-N. Hsiao, M. Sekine, and M. Hori, ACS Appl. Mater. Interfaces **15**, 35622 (2023).
[39]S.-N. Hsiao, N. Britun, T. Nguyen, M. Sekine, and M. Hori, ACS Appl. Electron. Mater. **5**, 6797 (2023).
[40]K. Shinoda, M. Izawa, T. Kanekiyo, K. Ishikawa, and M. Hori, Appl. Phys. Express **9**, 106201 (2016).
[41]M. Saito, H. Eto, N. Makino, K. Omiya, T. Homma, and T. Nagatomo, Jpn. J. Appl. Phys. **40**, 5271 (2001).
[42]Y. Kataoka, S.-I. Saito, and K. Omiya, J. Electrochem. Soc. **146**, 3435 (1999).
[43]J. E. Jung, Y. Barsukov, V. Volynets, G. Kim, S. K. Nam, K. Han, S. Huang, and M. J. Kushner, J. Vac. Sci. Technol. A **38**, 023008 (2020).
[44]P. A. Pankratiev, Y. V. Barsukov, A. A. Kobelev, A. Y. Vinogradov, I. V. Miroshnikov, and A. S. Smirnov, J. Phys.: Conf. Ser. **1697**, 012222 (2020).
[45]W. O. Lee *et al.*, Sci. Rep. **12**, 5703 (2022).
[46]A. Lii-Rosales, A. S. Cavanagh, A. Fischer, T. Lill, and S. M. George, Chem. Mater. **33**, 7719 (2021).
[47]D. M. Knotter, J. Am. Chem. Soc. **122**, 4345 (2000).
[48]J. Miller, Phys. Today **77**(8), 10 (2024).
[49]T. C. Allison, NIST-JANAF Thermochemical Tables—SRD 13 (2013).

18 November 2024 23:19:49

Published under an exclusive license by the AVS